ETH
Eidgenössische Technische Hochschule Zürich
Swiss Federal Institute of Technology Zurich

D PHYS
Laboratory for Solid State Physics
Quantum Device Lab

Semester thesis

Software for arbitrary single qubit & qutrit gate calibration

Author: Andreas Landig

Supervisor: Yves Salathe

Prof. Andreas Wallraff

November, 2013

Abstract

To implement a quantum processor, superconducting qubits in a circuit quantum electrodynamics architecture can be used. Due to fluctuations in its environment, parameters of the superconducting qubit or qutrit change on a long term basis. To run quantum algorithms on the processor, these parameters need to be known precisely. Thus, single qubit and qutrit operations have to be calibrated regularly. The more complicated the algorithm becomes, usually the more qubits are necessary to run it. Hence, it becomes unavoidable to execute the basic routines for the qubit or qutrit calibration automatically.
This thesis presents such a program for the automatic calibration of arbitrary single qubit and qutrit gates. For its implementation, *LabVIEW* and *Mathematica* are used.

Contents

Chapter 1

Introduction

One way to realize a quantum information processor is to use superconducting transom quantum bits (qubits) as artificial atoms that are coupled to a superconducting transmission line resonator. Such a solid state on-chip architecture, which is referred to as a circuit QED architecture, allows for the strong coupling of microwave modes inside the resonator to the qubit and thus for the exchange of coherent excitations between the qubit and the cavity [WSB+04]. Hence, quantum behavior can be observed in this macroscopic system in analog to a cavity QED system, where the qubit is a real atom and the resonator corresponds to an optical cavity.
Despite its decoupling from the environment, the superconducting artificial atom interacts with its environment. Among other things, these interactions result in a long-term change of parameters of the Hamiltonian describing the effective two level system (qubit) or three level system (qutrit). This necessitates the regular calibration of single qubit/qutrit gates. Empirically the calibration needs to be executed every twelve hours. If the calibration is done manually, it takes about 30 minutes for one qubit. In the *Quantum Device Lab*, recently a teleportation algorithm was implemented on a quantum processor with three qubits [SSO+13]. Considering the goal of realizing a large-scale quantum computer, the number of necessary qubits will be much larger. To realize for example a Grover algorithm, which searches a database with N entries for a desired entry, $\log_2 N$ qubits are necessary [Gro96]. Thus, automating the calibration of single qubit and qutrit gates becomes unavoidable. The implementation of a software for this purpose is the goal of this thesis.

The structure of the thesis is as follows: In Chapter 2, basic concepts of circuit quantum electrodynamics are introduced in order to understand how superconducting artificial atoms can be implemented, controlled and read out. In Chapter 3 the pulse sequences that are necessary for the characterization and calibration of the artificial atom are explained. In Chapter 4, the calibration program which was implemented during this thesis is explained in detail. This new software generalizes a previously written program for the automatic calibration of single qubit gates. Also, the improvements that have been done with respect to the previous version are highlighted. Finally, experimental results using the new calibration software are depicted and discussed in Chapter 5.

Chapter 2

Basics of circuit quantum electrodynamics

In this chapter, first the general theoretical concept behind a qubit/qutrit and the physical realization of such an artificial atom by using superconducting transmons is introduced. Also, single qubit/qutrit gates are explained. Consecutively, the coherent manipulation and readout of the state of the artificial atom in an circuit cavity quantum electrodynamics architecture is explained theoretically and experimentally.

2.1 Qubit/Qutrit

A qubit is an arbitrary quantum mechanical two level system. Its state vector

$$|\psi\rangle = \alpha\,|0\rangle + \beta\,|1\rangle = e^{\imath\gamma}\left(\cos\frac{\theta}{2}\,|0\rangle + e^{\imath\phi}\sin\frac{\theta}{2}\,|1\rangle\right)$$

can be represented by a unit vector on the Bloch sphere (see Figure 2.1), where α and β are complex numbers that fulfill $|\alpha|^2 + |\beta|^2 = 1$. $|0\rangle$ and $|1\rangle$ are the orthonormal basis states on the north and south poles of the sphere, which can be identified by the ground and excited state of the two level system. An arbitrary state of a qutrit, a three level system,

$$|\psi\rangle = \alpha\,|0\rangle + \beta\,|1\rangle + \gamma\,|2\rangle$$

with the normalization condition $|\alpha|^2 + |\beta|^2 + |\gamma|^2 = 1$ for the complex numbers α, β and γ cannot be represented on the Bloch sphere. However, if the population of the first excited state, the $|1\rangle$ state, is negligible compared to the populations of the ground and second excited states, it is convenient to map the system to an effective two level system, with $|0\rangle$ and $|2\rangle$ being the north and south poles. A build-up of population in $|1\rangle$ corresponds to a decay out of this two dimensional subspace, which reduces the length of the Bloch vector.
Using the Bloch sphere representation, one can easily visualize the time evolution of a two dimensional state vector in analogy to the time evolution of a spin 1/2 particle in a magnetic field. Thereby, one usually considers a frame which rotates at the transition frequency $\omega_{01} = \frac{1}{\hbar}(E_{|1\rangle} - E_{|0\rangle})$ about the quantization axis. In this frame, a magnetic field along an axis in the x-y plane, oscillating at the transition frequency, results in a rotation of the spin 1/2 particle around the field axis. As will be explained later, in the case of transmon qubits/qutrits, the oscillating magnetic field corresponds to a microwave signal on the charge line of the transmon.

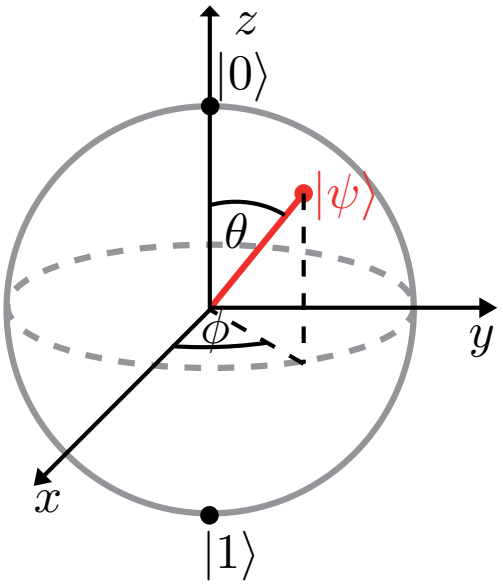

Figure 2.1: Bloch sphere representation of qubit.

A single qubit gate rotates the state vector of the qubit on the Bloch sphere. Thereby, any single qubit operation can be decomposed into a combination of rotations around the x and y axis [Bau12]. An operation that maps $|0\rangle$ to $|1\rangle$ and vice versa (NOT gate) corresponds to a rotation about an axis in the x-y plane by an angle of π. For the superconducting qubits, this can be realized by applying a resonant microwave pulse with the correct amplitude and duration - a so called π pulse. The exact rotation axis in the x-y plane is given by the phase of the pulse. One phase is defined to be the zero phase which corresponds to the x rotation axis [Bau12].
An arbitrary single qutrit gate can be decomposed into two single qubit gates, acting on the $|0\rangle$, $|1\rangle$ and $|1\rangle$, $|2\rangle$ subspaces, such that above formalism applies.

2.2 Transmon qubit

For the physical realization of qubits, macroscopic electrical circuits with nonlinear elements can be used. Thereby, Josephson junctions can serve as nonlinear elements. At low temperatures and sufficient decoupling from the environment, these circuits show quantum behavior with a discrete and anharmonic energy spectrum.
In the following, one possible circuit will be explained qualitatively. For a much more elaborate qualitative and also quantitative treatment, see [Bau12].

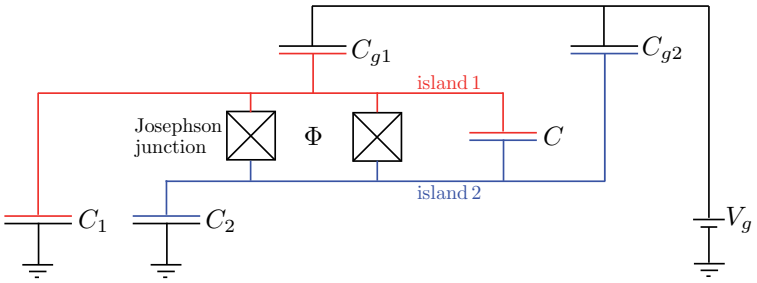

Figure 2.2: Schematic of superconducting transmon qubit.

The qubits which are currently used in the *Quantum Device Lab* at ETH Zurich are superconducting transmon qubits. As depicted in Figure 2.2, they consist of two islands, which are connected via two Josephson junctions and a capacitance C[1]. Thereby, the Josephson junctions form a loop (SQUID loop) which is penetrated by a magnetic flux Φ[2]. One can derive from a quantum mechanical treatment of the system [Bau12], that a finite energy is necessary to add a cooper pair to the island. This results in the desired anharmonic energy spectrum. To control the number of cooper pairs on the islands, the charge line is used, which connects the gate voltage V_g with the capacitance C_g. Consequently, a coherent manipulation of the qubit state can be realized by a coherent signal on the charge line.

2.3 Circuit quantum electrodynamics

The on-chip design of a transmon capacitively coupled to a coplanar waveguide resonator can be used for a non-demolition readout of the qubit state. The circuit QED architecture is schematically shown in Figure 2.3.

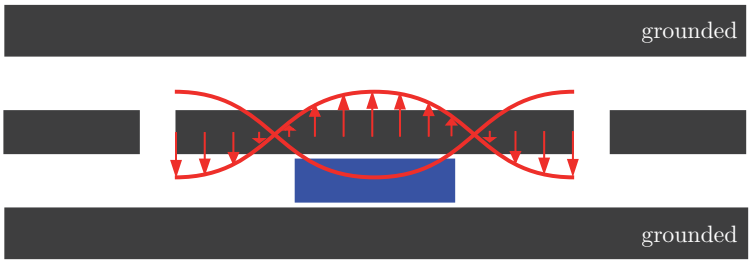

Figure 2.3: Circuit quantum electrodynamics architecture with coplanar waveguide resonator (gray) and superconducting qubit (blue). A standing wave (red) is formed in the resonator.

[1] This capacitance is used to reduce the qubit sensitivity to charge noise.
[2] The flux is used to control the transition frequency of the qubit.

The superconducting qubit is placed at an antinode of the standing wave in the resonator, to maximize the coupling strength. The system is then described by a Jaynes-Cummings type of Hamiltonian[3] [KYG+07]:

$$\hat{H} = \hbar \sum_j \omega_j \left|j\right\rangle \left\langle j\right| + \hbar\omega_r \hat{a}^\dagger \hat{a} + \left(\hbar \sum_i g_{i,i+1} \left|i\right\rangle \left\langle i+1\right| \hat{a}^\dagger + h.c. \right) \tag{2.1}$$

The first term describes the transmon qubit with energy levels $\hbar\omega_j$. The second term accounts for the quantized field mode in the resonator, within which a photon is annihilated (created) by $\hat{a}$ ($\hat{a}^\dagger$). The last term includes the strong coupling of the field mode to the transmon with $g_{ij} \propto V^0_{rms} \left\langle i\right| \hat{a}^\dagger \hat{a} \left|j\right\rangle$, where V^0_{rms} are the vacuum voltage fluctuations in the resonator.
In the dispersive limit, where the qubit is strongly detuned from the resonator, i.e. $|\Delta_0|, |\Delta_1| \gg g_{01}$, with $\Delta_i = \omega_{i,i+1} - \omega_r$, (2.1) can be transformed such that one arrives at [Bau12][4]

$$\hat{H} = \frac{\hbar}{2}\left(\omega_{01} + \frac{g^2_{01}}{\Delta_0}\right)\hat{\sigma}_z + \hbar(\omega_r + \frac{g^2_{12}}{2\Delta_1} + \chi\hat{\sigma}_z)\hat{a}^\dagger\hat{a}.$$

Besides the Lamb shift of the qubit transition frequency, also the resonance frequency of the resonator is shifted. As the sign of $\chi\hat{\sigma}_z$, where χ is the dispersive shift, depends on the qubit state, the dispersive regime can be used to perform quantum non-demolition measurements of the qubit state. Thereby one applies a coherent measurement tone to the resonator and measures the time dependent I and Q quadratures of the transmitted signal. A typical time trace, which is an average over 65.000 measurements of the same prepared state $\hat{\rho}$, can be seen in Figure 2.4.

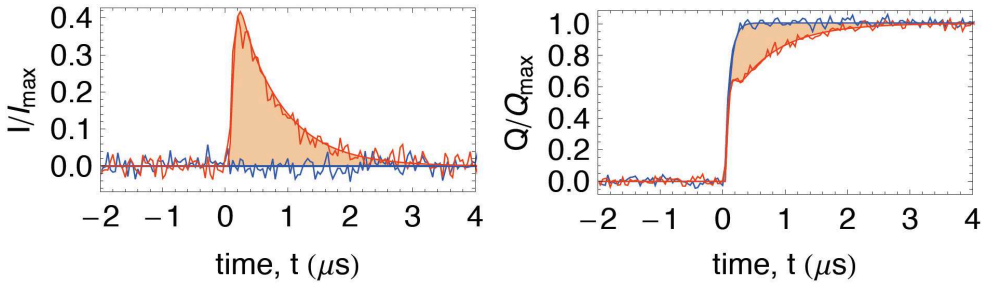

Figure 2.4: Time dependent resonator transmission quadratures I and Q (from [Bau12]). The ground state response is denoted in blue.

[3] The rotating wave approximation has been applied, allowing only for coupling terms that describe the excitation (de-excitation) of the qubit with the simultaneous annihilation (creation) of a photon in the resonator. For the most general form of the Hamiltonian, see [KYG+07].
[4] The ground and first excited state of the transmon is considered. Also, coupling to the second excited level is included. For a thorough derivation, see [Bau12].

The corresponding measurement operators are given as [Bau12]

$$\hat{\mathcal{M}}_{I,Q} = \alpha_0^{I,Q} |0\rangle \langle 0| + \alpha_1^{I,Q} |1\rangle \langle 1|$$

with $\alpha_i^{I,Q} = 1/N \int_0^T (\langle |i\rangle \langle i| \hat{\mathcal{M}}_{I,Q}\rangle - \langle |0\rangle \langle 0| \hat{\mathcal{M}}_{I,Q}\rangle) dt$ being the shaded area in Figure 2.4, that is integrated up to a time T. As $I(t), Q(t) = \mathrm{Tr}[\hat{\rho}\hat{\mathcal{M}}_{I,Q}]$, the qubit population can be extracted from the measurement by recording the response of the system to calibration pulses that prepare the qubit initially in the $|0\rangle$ or $|1\rangle$ state. To create these pulses, the correct amplitude and frequency has to be known in advance or one has to take an initial guess.
Above formalism can be extended to reconstruct the populations of a qutrit from the quadrature measurements. In this case, the non-demolition measurement operators are [Bia10]

$$\hat{\mathcal{M}}_{I,Q}(t) = s_0^{I,Q}(t) |0\rangle \langle 0| + s_1^{I,Q}(t) |1\rangle \langle 1| + s_2^{I,Q}(t) |2\rangle \langle 2|$$

where the $s_i^{I,Q}(t)$ are the known time traces for the quadratures when the qubit is in state $|i\rangle$. The quadrature signal for an arbitrary qutrit state $\hat{\rho}$ at measurement time step t_j is then given as

$$I(t_j), Q(t_j) = \mathrm{Tr}[\hat{\rho}\hat{\mathcal{M}}_{I,Q}(t_j)] = p_0 s_0^{I,Q}(t_j) + p_1 s_1^{I,Q}(t_j) + p_2 s_2^{I,Q}(t_j). \tag{2.2}$$

By fitting the measured trace (2.2) to a linear combination of the known pure state traces, the populations p_i and thus the qutrit state can be calculated. As for the qubit case, calibration pulses are used to obtain the pure state traces. However, for the three population readout, also the time trace of the $|2\rangle$ state needs to be recorded.
Compared to the reconstructed two-level populations, the standard deviation of the reconstructed qutrit populations is larger. Qualitatively this is because the three traces might not be fully linear independent. As the time trace depends on the detuning of the measurement tone from the resonator frequency, one can minimize this error by adapting the measurement detuning. For a more detailed treatment of this optimization, we refer to [Bia10].

2.4 Experimental setup

A strongly simplified version of the experimental setup, which is used to manipulate the superconducting artificial atom and to reconstruct its population, is depicted in Figure 2.5.
To coherently drive the qubit, the phase, frequency and amplitude of the microwave signal of the charge line at the gate capacitor needs to be controlled precisely. Therefore, an IQ-mixer is used. In an up-conversion process, the GHz local oscillator (LO) signal from a microwave generator at frequency ω_{LO} is mixed with two intermediate frequency (IF) signals on the I and Q input ports at frequency ω_{IF}, to generate a radio frequency output signal (RF output) at frequency ω_{RF}.[5]. For an ideal mixer and a phase shift of $\phi = \pi/2$ between the I and Q quadratures of equal amplitudes, one

[5] Typical frequencies: $\omega_{RF} \approx 6\,\mathrm{GHz}$, $\omega_{IF} \leq 100\,\mathrm{MHz}$

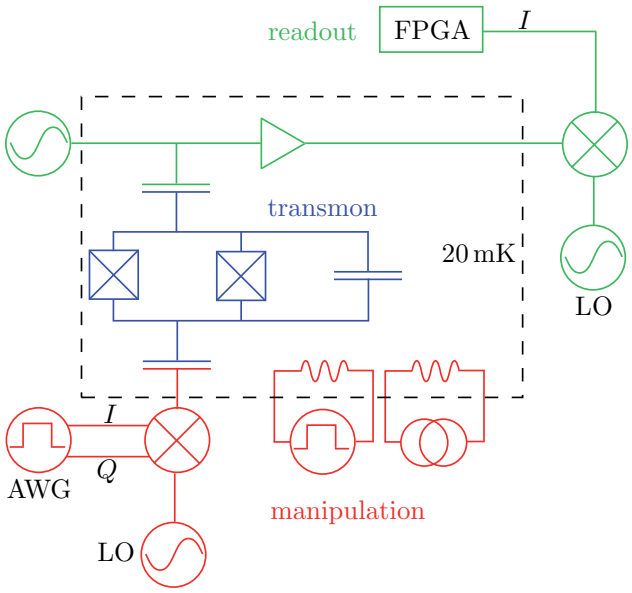

Figure 2.5: Simplified schematic of the experimental setup used for coherent single qubit and qutrit operations, according to [SSO+13]. Unless denoted otherwise, the components are at room temperature.

gets a single sideband at $\omega_{RF} = \omega_{LO} - \omega_{IF}$.[6] The desired RF signal control is achieved by adjusting the phase and amplitude of the signals at the IF input. The IF signals are generated using an arbitrary waveform generator (AWG). To perform a certain qubit operation (see Section 2.1), the signal from the AWG is a specific sequence of pulses (pulse pattern). Typically, the pulses within the pulse patterns are shaped in order to suppress unwanted frequency components. If for example a drive on the $|0\rangle \leftrightarrow |1\rangle$ transition also couples to the $|1\rangle \leftrightarrow |2\rangle$ transition, the second excited state will be populated. This not only results in a leakage out of the qubit subspace, but also in phase errors of the relative phase of the ground and first excited state during the pulse because the population of the second excited state introduces an AC Stark shift [Bau12].
One method that is used for pulse shaping is the so called derivative removal by adiabatic gate (DRAG). Thereby, the amplitude ϵ_Q of the Gaussian pulse on the Q input is optimized with respect to the amplitude ϵ_I of the Gaussian pulse on the I input according to [MGRW09]

$$\epsilon_Q(t) \propto q_{scale} \frac{\partial \epsilon_I(t)}{\partial t},$$

where q_{scale} is a scaling factor. To create the pulse patterns, which are loaded on the AWG, *Mathematica* scripts are used. Typically a sequence of pulse patterns is generated, which is as a

[6] Due to mixer imperfections, the output spectrum contains not only the desired sideband at $\omega_{LO} + \omega_{IF}$ but also leakage components at ω_{LO} and $\omega_{LO} - \omega_{IF}$. This can result in an unwanted qubit drive, which can be avoided by adjusting ϕ and the ratio of the quadrature amplitudes.

whole loaded on the AWG. The maximum number of patterns within a sequence is limited to the memory of the AWG. Note, that the calibration pulses necessary for the readout (see Section 2.3) are typically at the end of the sequence.
The scripts for pattern generation require parameters such as the pulse amplitude or the q_{scale} factor. These parameters are loaded from a so called pulse pattern configuration file.
Note, that in Figure 2.5 also the flux-bias lines are illustrated, which are used to change the qubit frequency. As this is not necessary for single qubit/qutrit operations, they will not be considered further in the thesis.

The readout of the transmon state using the resonator is challenging, as the resonator is populated only by a few photons. To get a processable signal, several amplifiers at different temperature stages are used. For details, we refer to the description of the cyrogenic wiring in [Bau12]. However, as it was stated in Section 2.3, to derive the transmon population via the time trace, the same experiment needs to be repeated for about 65.000 times. This can be avoided using a parametric amplifier, which allows for a single-shot read out of the transmon state (used for example in [SSO+13]). Note, that for the experimental data presented in Chapter 5, no single-shot readout was used.
The signal from the resonator is in a last step down-converted to an intermediate frequency (IF) by mixing it with a microwave local oscillator signal. Using digital down conversion (DDC) to downconvert the signal to 0 MHz, the signal quadratures are obtained.

Chapter 3

Pulse sequences for the calibration of arbitrary single qubit/qutrit gates

As it was explained in the Sections 2.1 and 2.4, to realize arbitrary single qubit/qutrit gates, pulses with the correct amplitude, duration, frequency and shape have to be applied to the charge line. Thus, several pulse parameters, i.e. parameters of the $|0\rangle \leftrightarrow |1\rangle$ and $|1\rangle \leftrightarrow |2\rangle$ transition, have to be determined.
The need for a controllable coherent manipulation of the $|1\rangle \leftrightarrow |2\rangle$ transition may not be clear at first glance. Arbitrary single qubit gates and a controlled NOT (CNOT) two qubit gate are known to form a universal set of quantum gates [BDD+02], i.e. a set of quantum gates with which any quantum algorithm can be implemented. In [DOS+12] an $\sqrt{\text{iSWAP}}$ was realized using two transmon qubits. As a CNOT gate can be generated using $\sqrt{\text{iSWAP}}$ and single qubit gates, [DOS+12] demonstrated the implementation of a universal set of quantum gates using transmon qubits. However, using qutrits can be advantageous, as it reduces the number gates necessary to implement a CNOT gate [Bau12]. This was first demonstrated in [DCG+09].

In the following, the pulse sequences to characterize qubits/qutrits for single gate operation are explained. Note, that calibration pulses (see Sections 2.4 and 2.3) are not stated explicitly.

3.1 Qutrit transition frequencies

A precise method to determine the $|0\rangle \leftrightarrow |1\rangle$ and $|1\rangle \leftrightarrow |2\rangle$ transition frequencies is to use a Ramsey pulse sequence (see Figure 3.1). In the qubit case a $\pi/2$ pulse at frequency $\tilde{\omega}_{0,1}$, which is slightly detuned[1] by $\omega_{det} = |\tilde{\omega}_{0,1} - \omega_{0,1}^{exp}|$ from the expected transition frequency $\omega_{0,1}^{exp}$, is used to create an equal superposition of the ground and excited state (the determination of the correct pulse amplitude is discussed below). Experimentally, one adjusts the IF frequency on the mixer input to get the detuned RF signal. In the rotating frame, the Bloch vector will then precess around the $\pm z$ axis with a frequency $\omega_{Ramsey} = |\tilde{\omega}_{0,1} - \omega_{0,1}|$. Where $\omega_{0,1}$ is the real frequency for the transitions. Note, that if the expected transition frequency is equal to the real transition frequency, $\omega_{Ramsey} = \omega_{det}$. After a time Δt, another off-resonant $\pi/2$ pulse is applied and the state of the qubit is measured.

[1] The detuning is typically a few MHz.

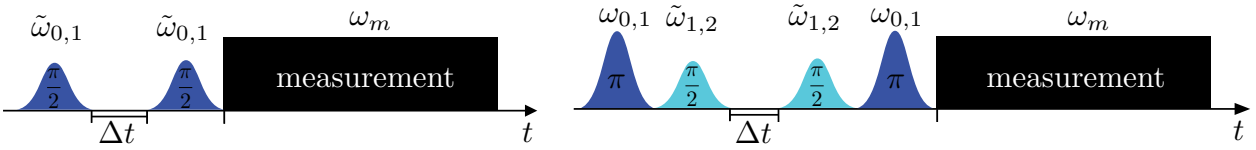

Figure 3.1: Schematic of Ramsey pulse sequence for $|0\rangle \leftrightarrow |1\rangle$ (left) and $|1\rangle \leftrightarrow |2\rangle$ (right) transition.

Depending on the delay Δt one will observe oscillations of the ground/excited state population at a frequency ω_{Ramsey}. Note that for a single run of the experiment, the sequence of patterns (see Section 2.4) are pulse patterns with different delays Δt. From the oscillation frequency one can then derive the transition frequency $\omega_{0,1}$. Since usually the detuning from the expected transition frequency is small, it is sufficient to adjust the frequency of the IF signal. The experimental results are discussed in [Men13].
To determine the $|1\rangle \leftrightarrow |2\rangle$ transition frequency, a similar pulse sequence is used. An initial π pulse at $\omega_{0,1}$, excites the qutrit to the $|1\rangle$ state. Then, as above, two separated $\pi/2$ pulses are used. However, they are now slightly off-resonant by $\omega_{det} = \tilde{\omega}_{1,2} - \omega_{1,2}$ from the $|1\rangle \leftrightarrow |2\rangle$ transition. Now, the idea is to map the qutrit to an effective two level system (see Section 2.1). This is achieved by another $|0\rangle \leftrightarrow |1\rangle$ π pulse. As for the qubit case, coherent oscillations depending on Δt are expected, from which $\omega_{1,2}$ can be extracted (see Section 5.1).

3.2 Qutrit transition frequencies for large detuning of the drive

The situation for the Ramsey measurement as described above is schematically depicted in Figure 3.2. Experimentally, a detuning ω_{det} from the expected transition frequency $\omega_{0,1}^{exp}$ is set and oscillations at a frequency ω_{Ramsey} are recorded. For large detuning of the drive from the real transition frequency, i.e. $\omega_{Ramsey} > \omega_{det}$, one can in general not extract from the measured oscillations whether the real transition frequency is above or below the drive frequency (see left and right scheme in Figure 3.2). One method to derive this sign information from the measurement is to apply the $\pi/2$ pulses in the sequence of Figure 3.1 about different axes, for example the first one about the x and the second one about the y axis. Then, the slope of the oscillations at $\Delta t = 0$ contains the sign information [Bau12]. However, if a two population readout is used for the measurement on the $|1\rangle \leftrightarrow |2\rangle$ transition, this scheme is more difficult to apply since one has to take into account the phase of the pulse which is used to drive the $|0\rangle \leftrightarrow |1\rangle$ transition.

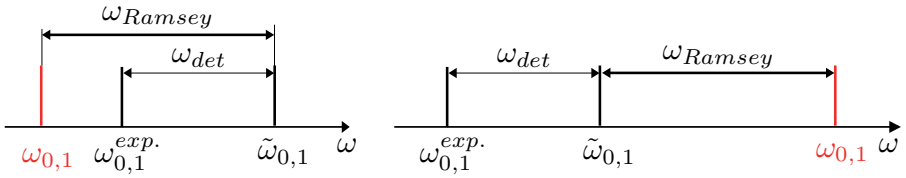

Figure 3.2: Schematic of frequencies involved in Ramsey measurement. The measured ω_{Ramsey} is the same for the left and right scheme.

An alternative method to derive the sign information, which works for all above cases, is to do two subsequent Ramsey measurements with two different detunings. It can easily be calculated, that in order to be consistent with the data for both detunings, only one of the two cases in Figure 3.2 is possible. The analysis of such a measurement will be demonstrated in Section 5.1.

3.3 Pulse amplitude

To do a specific rotation of the Bloch vector, the correct amplitude and duration of the pulse on the charge line has to be known. These pulse parameters are determined using Rabi oscillations (see Figure 3.3).

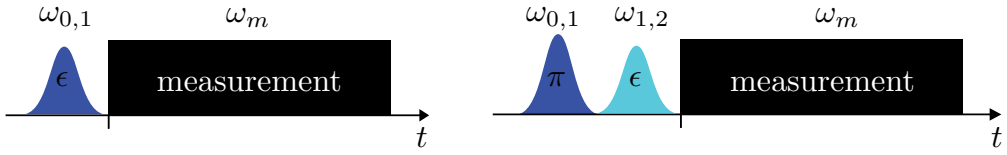

Figure 3.3: Schematic of Rabi pulse sequence for $|0\rangle \leftrightarrow |1\rangle$ (left) and $|1\rangle \leftrightarrow |2\rangle$ (right) transition.

Thereby, the qubit is driven with a resonant pulse of fixed duration but variable amplitude ϵ. Note, that the sequence of pulse patterns for a single run of the experiment contains patterns with variable ϵ. The measured populations will then show coherent oscillations, from which the amplitudes of the π and $\pi/2$ pulses for the $|0\rangle \leftrightarrow |1\rangle$ transition can be extracted. This analysis is described in [Men13].
In the same manner, the amplitudes for the π and $\pi/2$ pulses of the $|1\rangle \leftrightarrow |2\rangle$ transition can be determined by driving this transition with a pulse of variable amplitude (see section 5.2 for data analysis). Compared to the qubit case, an additional initial π pulse on the $|0\rangle \leftrightarrow |1\rangle$ transition is necessary to populate the first excited state.

3.4 DRAG parameter

As it was discussed in Section 2.4, DRAG pulses minimize phase errors. In order to obtain the optimal value of q_{scale}, a pulse sequence which is highly sensitive to phase errors is used (see Figure 3.4).

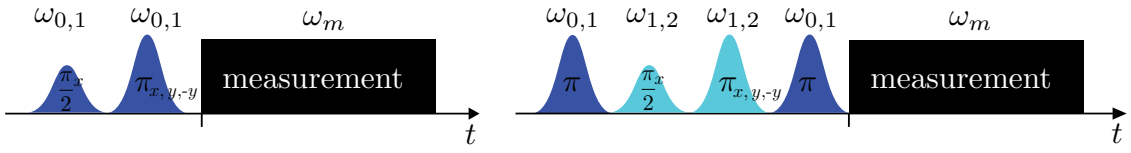

Figure 3.4: Schematic of pulse sequence to determine the DRAG pulse parameter q_{scale} for $|0\rangle \leftrightarrow |1\rangle$ (left) and $|1\rangle \leftrightarrow |2\rangle$ (right) transition.

The pulse sequence for the $|0\rangle \leftrightarrow |1\rangle$ transition consists of a $\pi/2$ pulse about the x axis followed by a π pulse about the x,y or -y axis. For an optimal value of q_{scale}, all three sequences result in the same final state, which is an equal superposition of ground and excited state. However, if the scaling parameter differs from the optimal value, phase errors due to leakage out of the qubit subspace introduce deviations, which are measurable as deviations from the expected population of 1/2. Experimental data in which q_{scale} is varied is discussed in [Men13].
To determine the optimal DRAG parameter for the $|1\rangle \leftrightarrow |2\rangle$ transition, an initial π pulse excites the qutrit to the $|1\rangle$ state. Then, the same pulse sequence as for the qubit is used on the $|1\rangle \leftrightarrow |2\rangle$ transition. Finally, a π pulse maps the qutrit to an effective two level system. For an optimal value of q_{scale}, the expected population of $|2\rangle$ is 1/2. Experimental data used to extract this optimal value is shown in Section 5.3.

After executing above pulse sequences for multiple times, the $|0\rangle \leftrightarrow |1\rangle$ and $|1\rangle \leftrightarrow |2\rangle$ transitions should be calibrated. In order to check whether the calibration was successful, combinations of pulses with different amplitudes and phases are used. This pulse sequence will further be denoted by *CalTom*.

3.5 Energy relaxation time T_1

For the usage of superconducting qubits/qutrits to implement quantum algorithms, it is necessary to determine how many gate operations can be performed before the decoherence in the system becomes too large. Thus, it is necessary to determine the energy relaxation time T_1 for the system initially prepared in the $|1\rangle$ and $|2\rangle$ state. Due to coupling of the artificial atom to the environment, the populations of these states will decay to $1/e$ of the initial population after a time $T_{1,1}$ and $T_{1,2}$, respectively. To determine these times, the pulse sequences in Figure 3.5 are used.
For the qubit, the system is prepared in $|1\rangle$ using a π pulse. After a variable time Δt, the population in $|1\rangle$ is measured. From the time dependent population, $T_{1,1}$ can be extracted.
For the qutrit, also the energy relaxation time of the population initially in $|2\rangle$ has to be measured. Thus, the system is excited with a π pulse on the $|0\rangle \leftrightarrow |1\rangle$ followed by a π pulse on the $|1\rangle \leftrightarrow |2\rangle$ and the $|0\rangle \leftrightarrow |1\rangle$ transition. The last π pulse is to project the system to the effective two level system $|0\rangle$, $|2\rangle$. As for the qubit, the energy relaxation time can be investigated with a delayed measurement.
Experimental results will be discussed in Section 5.5.

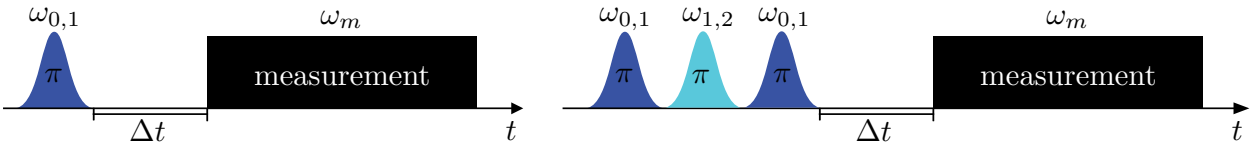

Figure 3.5: Schematic of pulse sequence to determine the energy relaxation time for the $|1\rangle$ (left) and $|2\rangle$ (right) state.

Chapter 4

Calibration software

In Chapter 1 the need for a software for automatic calibration of single qubit and qutrit gates was explained. The pulse sequences that need to be executed by the software were presented in Chapter 3.
In this Chapter I first present a software for the automatic calibration of single qubit gates, which was already implemented when I started my project. Also, its disadvantages are discussed. Then, a new program for the automatic calibration of arbitrary single qubit and qutrit gates, which was implemented during my thesis, is introduced. This includes the presentation of a new data flow, a new graphical interface and additional features of the new calibration program.

4.1 Previous version of the calibration software

The calibration program presented in this thesis is based on a software of Jonas Mlynek and Tim Menke [Men13]. This software was designed for the automatic calibration of single qubit gates. Thus, as explained in Sections 3.1 to 3.4, the software determines amplitudes of the π and $\pi/2$ pulses, the IF frequency and the DRAG pulse parameter q_{scale} for the $|0\rangle \leftrightarrow |1\rangle$ transition by executing certain calibration routines (e.g. Ramsey pulse sequence).

Figure 4.1: Typical sequence of routines for the calibration of the $|g\rangle \rightarrow |e\rangle$ transition.

A sequence of routines that is typically used for the calibration of the transition can be seen in Figure 4.1. All routines consist of similar steps that need to be executed successively. In Figure 4.2, the most general schematic of these steps is depicted.
As it was explained in Section 2.4, the parameters necessary to create pulse patterns are stored in a pulse pattern configuration file. With *Mathematica* scripts, these parameters are extracted and used to create the pattern files for a certain pulse sequence. For the communication with the experimental setup, the visual programming software *LabVIEW* is used. With this software, the patterns are loaded on the AWGs, the measurement is performed and the measured data is saved. In the last step, the data is analyzed using *Mathematica* scripts and new parameters such as new π and $\pi/2$ amplitudes are saved in the pulse pattern configuration file.

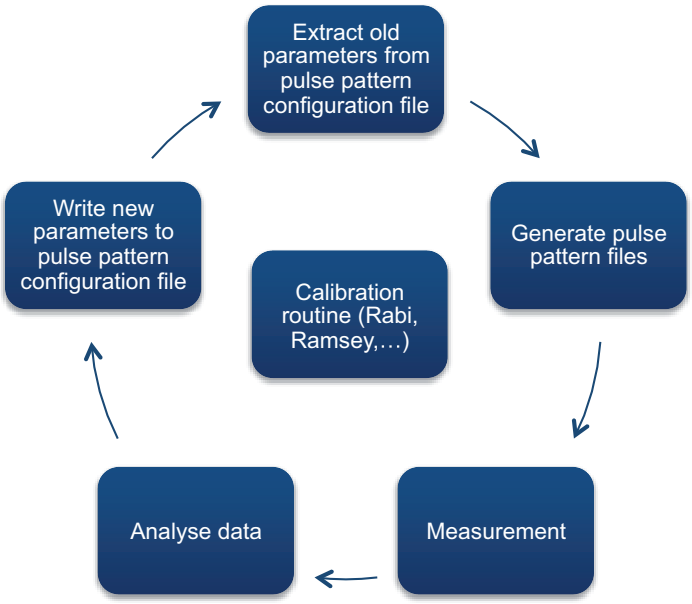

Figure 4.2: Schematic of calibration steps of previous version.

To understand the calibration software in detail, the corresponding data flow is shown in Figure 4.3. Note, that the data flow is depicted for a single run of one calibration routine within a sequence of routines.
The data flow can be separated into a *Measurement* and a *Pattern generation & data analysis* part (see color code in Figure 4.3).

In the measurement part, two main VIs[1] are executed. To run a calibration sequence, a multitude of parameters need to be specified. These include calibration sequence specific parameters and other fixed parameters, such as the frequencies of the LO drives or calibration settings of the mixers. All parameters are contained in the *Cleansweep configuration template* file. For every run of a calibration routine within the sequence, the variable parameters are modified by the VI *QubitCalib main*. Before running the calibration sequence, the user needs to specify within the graphical interface of this VI the desired calibration sequence (for example according to 4.1) and define necessary paths (for example the location of the *Mathematica* pattern generation and data analysis scripts). Also, experiment-specific physical parameters for the drive and readout of the artificial atoms need to be set (for example the physical channels of the AWG for the I/Q quadratures of the IF input). For details about this VI we refer to [Men13].
The updated parameters are then used to execute the VI *CleanSweep*. This VI directly runs the experiment. Thus, among other things it loads the pulse pattern files on the AWGs and sets the FPGA, which processes the experimental data.

[1] A *LabVIEW* program is called virtual instrument (VI).

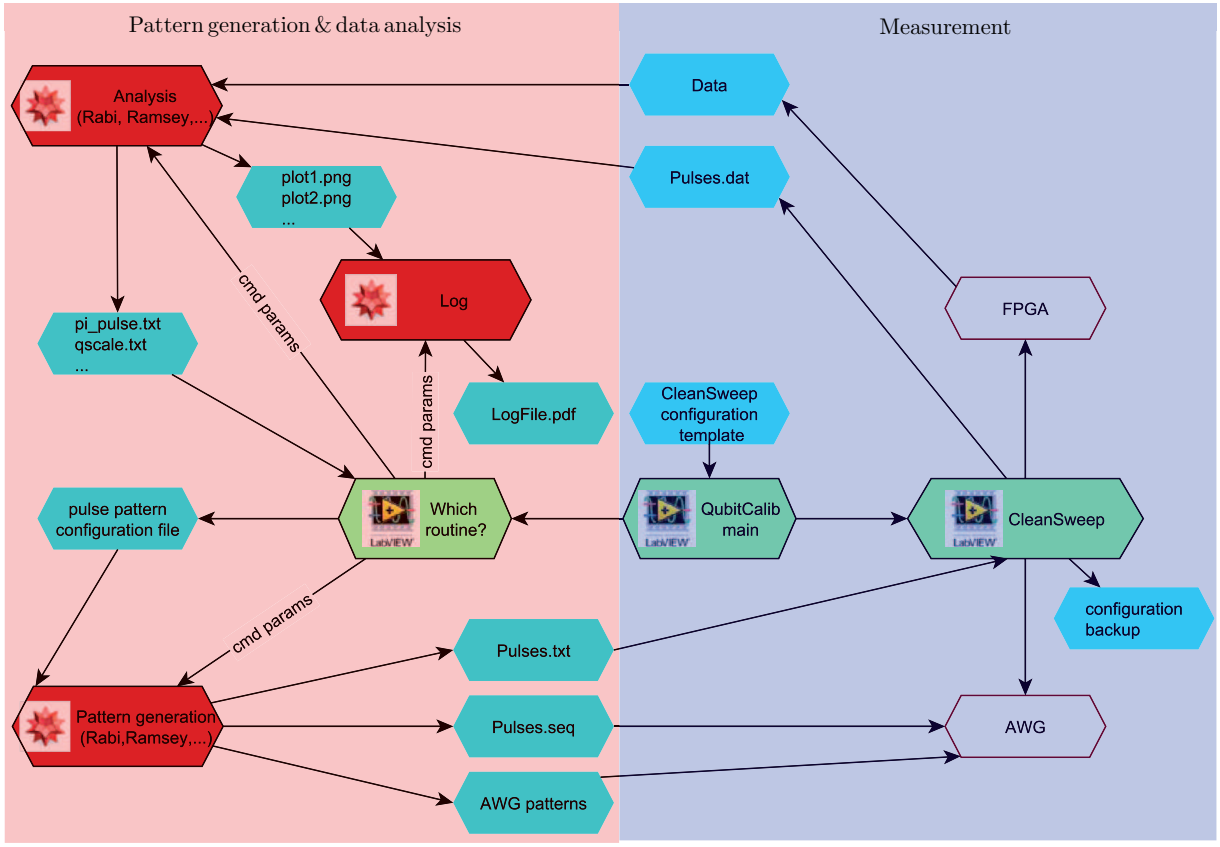

Figure 4.3: Data flow of the previous version of the calibration software illustrated for a single run of one calibration routine. Files are denoted in blue.

In the *Pattern generation & data analysis* part, the *Mathematica* scripts for the pattern generation, data analysis and the generation of a log file are executed. This part also contains subprograms (subVIs) of the *QubitCalib main* VI. Depending on the calibration routine, different routine-specific separate subVIs are executed. These subVIs thus act as a "which routine filter".
Using *LabVIEW*, the analysis and pattern generation scripts are run via the *Windows* command line. Thereby, the command to execute the scripts contains for example the path of the measurement data. The script for the data analysis saves new calibration parameters, such as a new value of q_{scale} in a text file. Using routine specific *LabVIEW* VIs, these parameters are written to the pulse pattern configuration file and shown on the graphical interface of *Qubit Calib main*. Note, that a backup of the pattern configuration file is created before every routine, such that if needed the old parameters can be recovered. The analysis script also exports a .png file with plots of the experimental data and the new parameters. The file name contains an index, that marks the number of the calibration routine within the sequence. Using this index, a *Mathematica* log file script exports the merged .png files as a .pdf file and deletes initial files.

The pattern generation script extracts the pulse parameters from the pulse pattern configuration file and creates three different files. The .seq file can be read by the AWG and describes the pattern. The *AWG patterns* are binary files that contain integers representing the time dependence of the signal amplitude. The text file is a copy of the pulse pattern configuration file with a few parameters added that describe the pattern, such as the total number of patterns within a sequence of patterns.

4.2 Disadvantages of the previous version

The goal of this thesis is to implement a software for the automatic calibration of arbitrary single qubit and qutrit gates. Therefore, one important feature of this software should be that new single qubit and qutrit gates can easily be added. With "easy" we mean, that there is no need for *LabVIEW* programming. The user only has to write *Mathematica* scripts for pattern generation and data analysis. For the software described in Section 4.1, new single qubit/qutrit gates cannot be added easily, as there are routine specific separate subVIs of *QubitCalib main*. If one for example wants to add a routine that determines a new parameter (for example π pulse amplitude for $|1\rangle \leftrightarrow |2\rangle$ transition), new subVIs have to be implemented that among other things extract this parameter from the text file and write it to the pattern configuration file (see Figure 4.3).
In the previous version, also no proper handling for *Mathematica* errors is implemented. An error occurs if for example the experimental data cannot be fitted properly in the analysis scripts. In this case the user might want *LabVIEW* to continue with the next calibration routine instead of aborting the whole calibration sequence.

4.3 New version of the calibration software

4.3.1 Data flow

A new version of the calibration software that does not have the disadvantages explained in Section 4.2 is based on the data flow in Figure 4.4.
Instead of the routine dependent subVIs and the text files, a .ini file and the standard output of *Mathematica* is used together with a new version of the *QubitCalib main* VI. Also, the analysis scripts directly write new parameters to the pulse pattern generation file.

For every routine during a calibration sequence, the .ini file is created by *LabVIEW*. It contains all parameters necessary to run both the analysis and pattern generation scripts. An excerpt from such a file is shown in Figure 4.5. The content is divided into sections which have a label in square brackets at their beginning. The parameters of the first section are the index of the current routine, which is needed to create the log file (see Section 4.1), and a user controlled boolean, that specifies whether the pattern configuration file shall be updated. The second section contains all paths that are specified in the graphical user interface in Figure 4.7 (this interface is explained in detail below) as well as the data saving folder and the number of the measurement within this

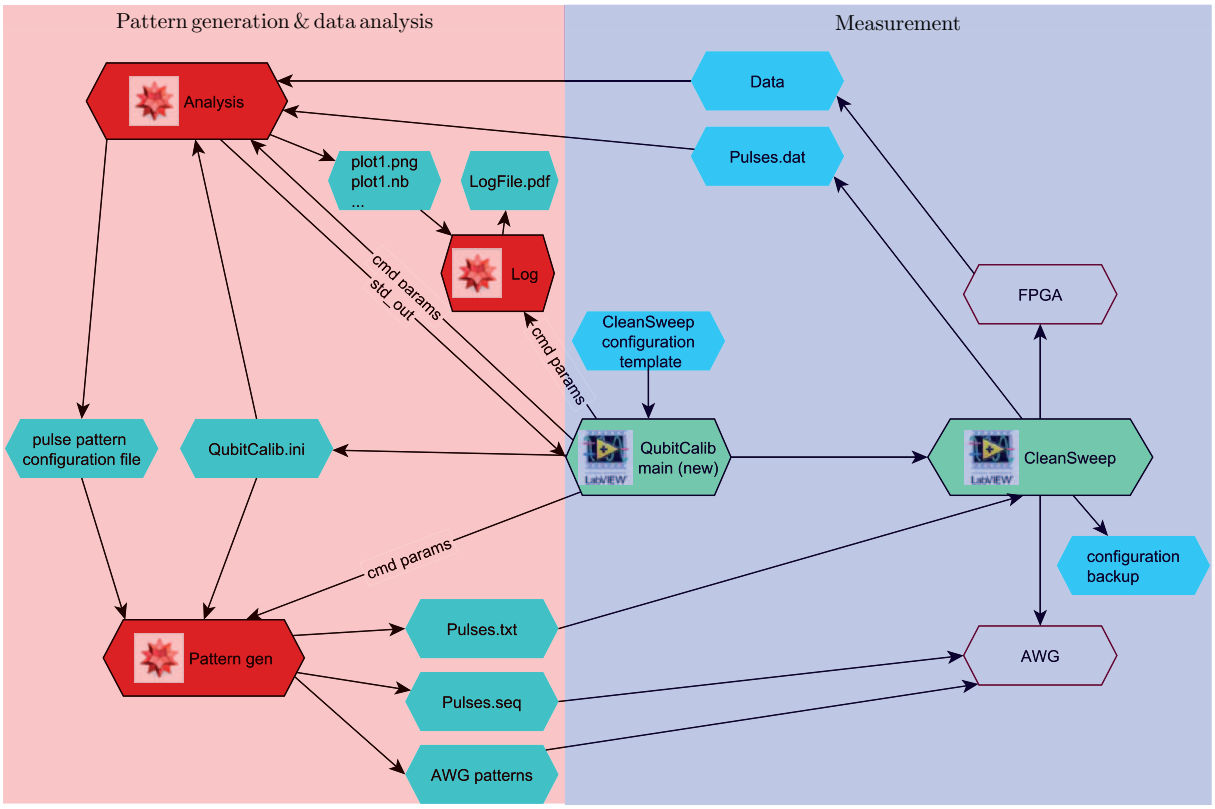

Figure 4.4: Data flow of the new version of the calibration software illustrated for a single run of one calibration routine. Files are denoted in blue.

```
[TmpParameters]
LogFileIndex = "1"
UpdateConf = "TRUE"

[CalibrationPathCluster]
DataStorage.Filenumber = "1095"
DataStorage.DataSavingFolder = "/C/dataC/130201"
...

[MeasChannelArrayElement]
UpconvChPair = "3"
UpconvLO = "4"
...
```

Figure 4.5: Excerpt from the .ini file.

folder. The last section contains setup specific qubit settings, which are explained in item 1 below. The path of the .ini file is read in via the command line. The white space separated strings in the command line input are parsed by *Mathematica* as a list of strings. The path and name of the .ini file needs to be the last string and is read in as follows:

```
qubitCalibIniFileName=FileNameTake[Last[$CommandLine]];
qubitCalibIniFilePath=DirectoryName[Last[$CommandLine]];
```

Then, the .ini is initialized as a list of strings using

```
calibIni=LoadConfigFile[qubitCalibIniFilePath,
qubitCalibIniFileName,rules->False]];
```

Thereby, .ini section names in square brackets are appended with points to variable names within the section. A possible string in the list calibIni is for example "TmpParameters.UpdateConf = "TRUE"". Finally, the value of the parameters within the list can be assigned to a variable. Defining a variable like

```
updateConfig=GetConfigParam[calibIni,"TmpParameters.UpdateConf"]
```

would assign the string "TRUE" to the variable.

Compared to the previous version, the standard output of the *Mathematica* analysis script is used. This output is parsed line by line using *LabVIEW* and the value of labels are extracted as strings. Thereby, labels are the first white-space separated strings in a line. This feature was implemented by Johannes Heinsoo. For details we refer to his semester thesis. The standard output is used for error handling and to show the new values from the data analysis. Also the difference of the parameter values before and after the analysis is printed in a status box on the graphical interface of *QubitCalib main* (see Figure 4.6). The corresponding strings for the labels are "new_values", "delta_values" and "ErrorMsg". These labels have to be used in the *Mathematica* script. Note, that if the label "ErrorMsg" does not exist in the standard output, it is treated as an error. A string can be written to the standard output using the function

```
StdOutput[string_]:=WriteString[$Output,string<>"\n"];
```

In *LabVIEW* error handling is implemented such that parameter values are only shown if the error message is the string "none". In such a case, the output in *LabVIEW* can look as follows:

```
new_values -> pi_amp_ef=0.617816 pihalf_amp_ef=0.309253
delta_values -> delta_pi_amp_ef=-0.024904 delta_pihalf_amp_ef=-0.014216
```

If the error message is not "none" the error is handled as a soft error. This means that *LabVIEW* is not aborted but the next calibration routine within the sequence is executed. Also a message like

```
The last operation had following user defined soft error (6010):
IF frequency could not be fitted. This pattern config parameter is
unchanged.
Continuing with next operation.
```

is displayed in the status box. The number in parentheses is the error code, which specifies whether the error is a soft or a hard error. In case of a hard error, *QubitCalib main* is aborted. If for example the path to the *Mathematica* scripts for a certain activated calibration routine does not exist, it is considered as a *LabVIEW* hard error. Hard and soft errors are distinguished according to their error code. The ranges for the codes of soft and hard errors as well as all used error codes are defined in the file "error_codes.txt" in the "QubitCalib" main directory.

For the new data flow, new parameters are directly written from the analysis scripts to the pattern generation files. This feature was implemented with the function ReplaceParameterInConfFile in *Mathematica* by Markus Oppliger. Thereby, the function also checks if the value of the parameter to be updated is a numerical value. Thus, if for example the fit did not work properly, the pulse pattern configuration file will be left unchanged.

The creation of the log files is very similar to the previous version. However, in addition to the temporary .png file, the analysis scripts export a temporary *Mathematica* notebook with the important plots and the new as well as the old calibration parameters. The log file script then merges the notebooks, creates a .pdf file and deletes the temporary files. The implementation of a new log file handling was necessary, as for more than five calibration routines within a sequence, the analysis PC ran out of RAM when executing the log file script.

4.3.2 Graphical interface

Besides the generalization of the *QubitCalib main* VI in order to implement the new data flow, also the graphical interface changed, as new features were added. For a detailed description of the previous interface, we refer to [Men13].
The modified graphical interface is shown in Figure 4.6 and Figure 4.7. Both parts of the interface can be accessed using a tab control.
Note, that *QubitCalib main* was also extended for the calibration of certain two qubit gates. The lower left part in Figure 4.6 is used for the settings to calibrate these gates. For more information we refer to the semester thesis of Johannes Heinsoo.
The procedure to start the calibration using the new interface shown in Figure 4.6 and 4.7 is as follows:

1. The user sets setup specific settings for the qubit/qutrit pulses.
   Each physical qubit/qutrit that is activated (calibrate on/off button) is assigned to a channel pair of the AWG, that is used to drive it. Also, the channel indices of the microwave generators for up- and down-conversion as well as for the resonator drive need to be specified. Note, that the assignment of a channel index to the channel of a physical device (AWG, microwave generator) is done in *CleanSweep*. To increase the fidelity of the readout, the parametric amplifier can be switched on. Further, the channel on the FPGA for the acquisition of data and the format of the data (for example $I_1 + \imath Q_1$) has to be set. Note, that also the flux line

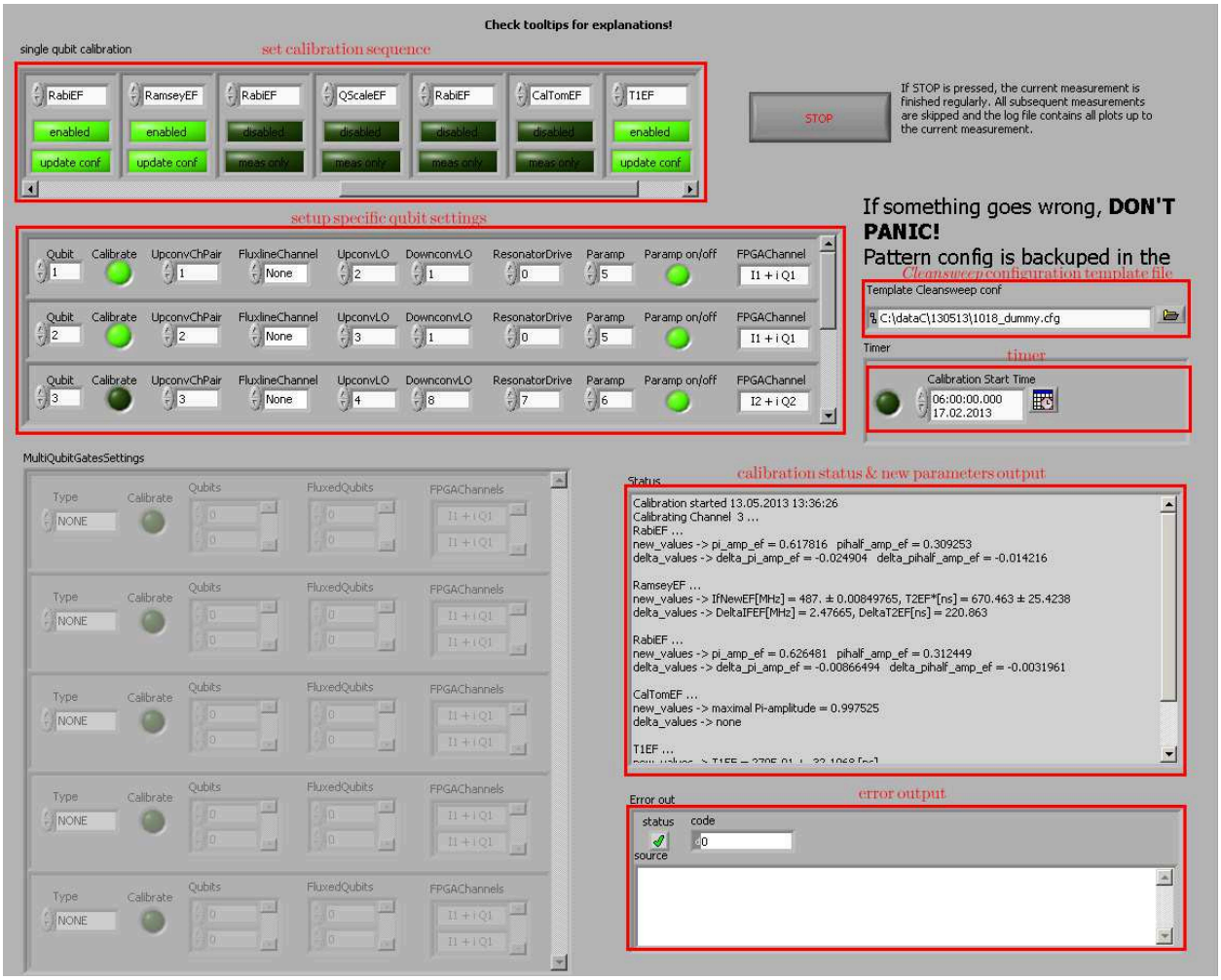

Figure 4.6: Graphical user interface part I for new version of the *QubitCalib main* VI.

for a qubit/qutrit can be specified. However, this is not necessary for single qubit or qutrit gates.

2. The following paths have to be set in the part of the interface in Figure 4.7:
   - **General paths:** To execute the mathematica scripts, the path to the *Mathematica* kernel has to be entered. Also, the path where the notebooks that are merged by the log file script are saved temporarily needs to be specified.
   - **Data storage:** The user has to specify the root directory. In this directory, a folder, which is named after the date of the measurement, is created automatically [Men13]. Within this folder, the experimental data, the .ini file and a screenshot of the graphical

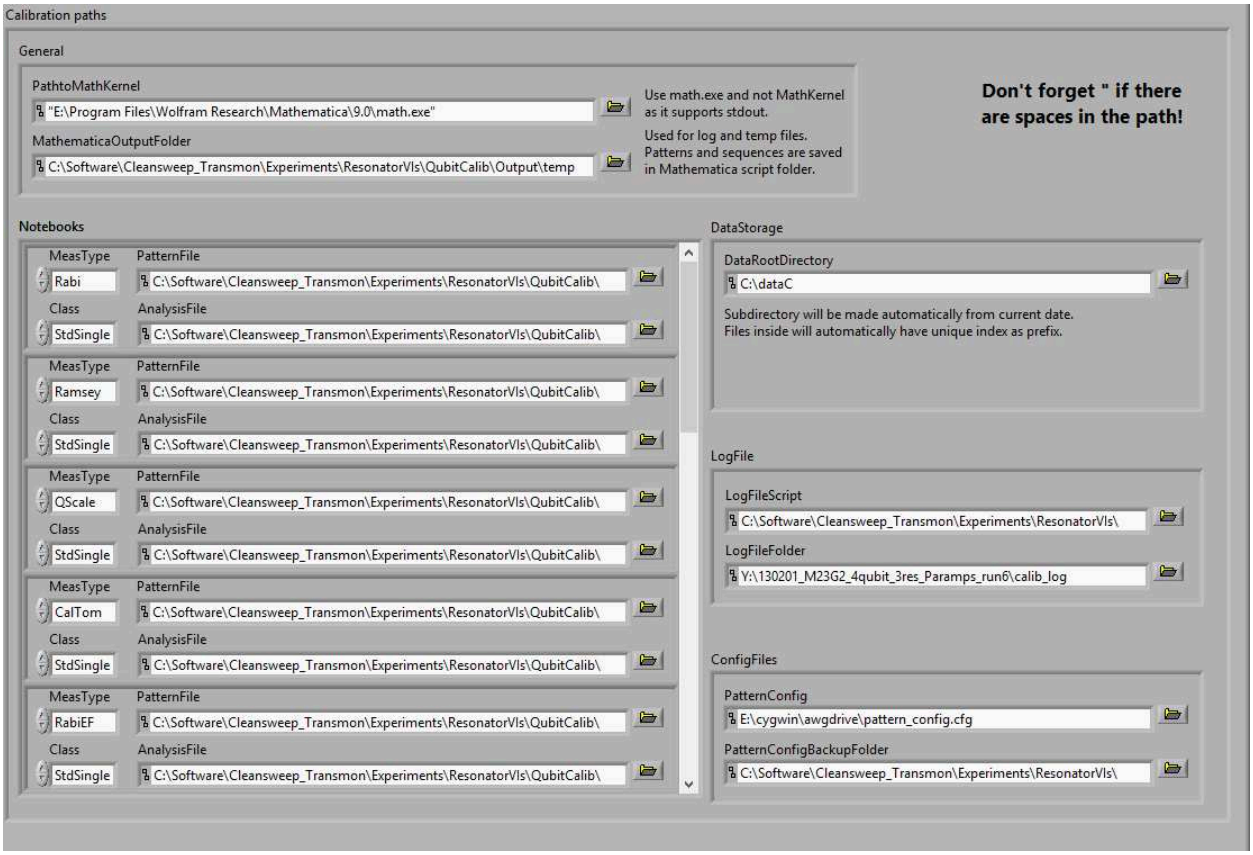

Figure 4.7: Graphical user interface part II for new version of the *QubitCalib main* VI.

interface of *Cleansweep* will be saved. The names of these files contain a file number, which is consecutive during a measurement day.

- **Log file:** The path to the log file script and the directory where the log files are saved is defined.
- **Configuration files:** The path to the pattern configuration file and the directory for the backup of the configuration file has to be entered.
- ***Mathematica* scripts**: For every calibration routine, the path to the pattern generation and analysis script needs to be set. Also, the name and type (single or multi qubit gate) of the routine has to be choosen.

3. The user specifies the calibration sequence.
   In the upper left part in Figure 4.6, the sequence that shall be executed can be set by enabling or disabling certain routines. The user can also choose whether new parameters gained from the data analysis shall be written to the pattern configuration file.

4. The user specifies the path to the configuration template file of *Cleansweep* and can set a time and date for the measurement to start (see middle right part in Figure 4.6).

When *Qubit Calib main* is executed, the sequence of activated calibration routines will run successively for the activated qubits/qutrits. The status of the calibration can be extracted from the status box in Figure 4.6, which is updated after every routine. There, the qubit/qutrit that is about to be calibrated, the name of the current routine, and the values of the desired labels in the standard output (see Section 4.3.2) are displayed.

In addition to the above mentioned new features of the calibration software, the following features were programmed during the semester thesis:

- The pattern generation and analysis scripts for the calibration of the $|1\rangle \leftrightarrow |2\rangle$ transition were implemented. There are analysis scripts for either two or three population readout (see Section 2.3).
- The Ramsey measurement for large detuning is implemented.
- The energy relaxation times $T_{1,1}$ and $T_{1,2}$ can be determined.
- The pattern generation and analysis scripts no longer contain hardcoded experimental parameters like the minimum and maximum value of the pulse amplitude ϵ for a Rabi measurement. These parameters are now extracted from the pulse pattern configuration file, where they can easily be specified for every AWG channel pair.
- If the calibration parameters determined by the analysis script are no numerical values, an error message is created, that is displayed in the standard output (according to Section 4.3.1). Also the pulse pattern configuration file is not updated.
- The dephasing time T_2^* (see Section 5.1) is added to the pulse pattern configuration file.

Chapter 5

Experimental results

In Chapter 4, a new software for the automatic calibration and characterization of superconducting qutrits was presented. As explained in Chapter 3, this program uses different routines for the calibration. Compared to the previous version of the software (see Section 4.1), new routines were added. In the following, the automatic analysis of experimental data from running these routines is explained and experimental results are presented. The experiments were performed on one transmon qutrit on a sample consisting of three qutrits and two coplanar waveguide resonators (see [SSO+13]). Using the flux line, the qutrit was operated at a $|0\rangle \leftrightarrow |1\rangle$ transition frequency of $\omega_{0,1}/2\pi = 6.342\,\text{GHz}$. The absolute anharmonicity was $\alpha \cong E_C/h = 0.287\,\text{GHz}$, where E_C is the charging energy. It was coupled with a strength of $g/2\pi = 0.240\,\text{GHz}$ to a coplanar waveguide resonator. The resonator had a resonance frequency of $\omega_r/2\pi = 9.677\,\text{MHz}$ and a decay rate of $\kappa/2\pi = 2.5\,\text{MHz}$. For the coherent drive, the $|0\rangle \leftrightarrow |1\rangle$ and $|1\rangle \leftrightarrow |2\rangle$ pulses had a width of $\sigma = 3\,\text{ns}$ and $\sigma = 5.5\,\text{ns}$, respectively.
Note, that all routines that were implemented for the previous version of the calibration software were successfully tested on the sample using the new version. As the same experimental data as in [Men13] was obtained, these experimental results will not be presented.

5.1 $|1\rangle \leftrightarrow |2\rangle$ transition frequency

As it was explained in Section 3.1, for a Ramsey pulse sequence one expects oscillations of the populations as a function of the delay Δt. Using a coherent drive with a detuning of 4 MHz from the $|1\rangle \leftrightarrow |2\rangle$ transition, the experimental data in Figure 5.2 was obtained. For the data analysis, the three level population reconstruction according to Section 2.3 was used. As the qutrit is mapped to an effective two level system of $|0\rangle$ and $|2\rangle$, Ramsey fringes for these two populations are observed. However, there is also a decay out of this two dimensional subspace, as the population of the first excited state (see red points in Figure 5.2) increases due to energy relaxation from the second excited state. This decay can also be observed in the oscillating populations, which decrease on average.
If the experimental data is instead analyzed using the two population readout, the experimental results for the time dependence of the $|2\rangle$ population are different. For this analysis method, only the response of the system in the states $|0\rangle$ and $|2\rangle$ is known. Populations in $|1\rangle$ and $|2\rangle$ consequently cannot be distinguished and the population of $|1\rangle$ is wrongly considered as a population of $|2\rangle$. Consequently, in contrast to the three level readout (see blue points in Figure 5.2), the population of $|2\rangle$ seems to increase on average. Therefore, if the decay out of the qubit subspace is not negligible (see Figure 5.2), three level population readout has to be used to get physically plausible results.

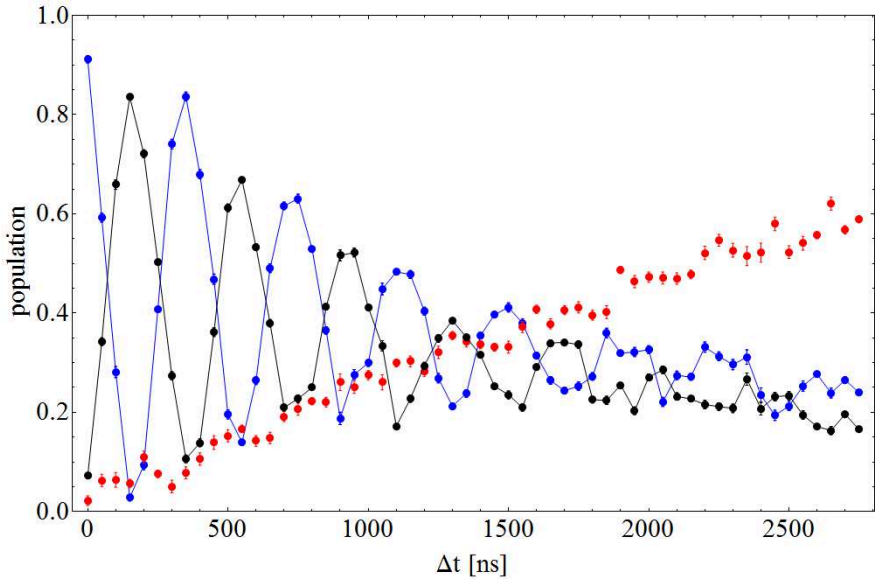

Figure 5.1: Three level population readout of Ramsey routine with the ground (black), first excited (red) and second excited (blue) state populations.

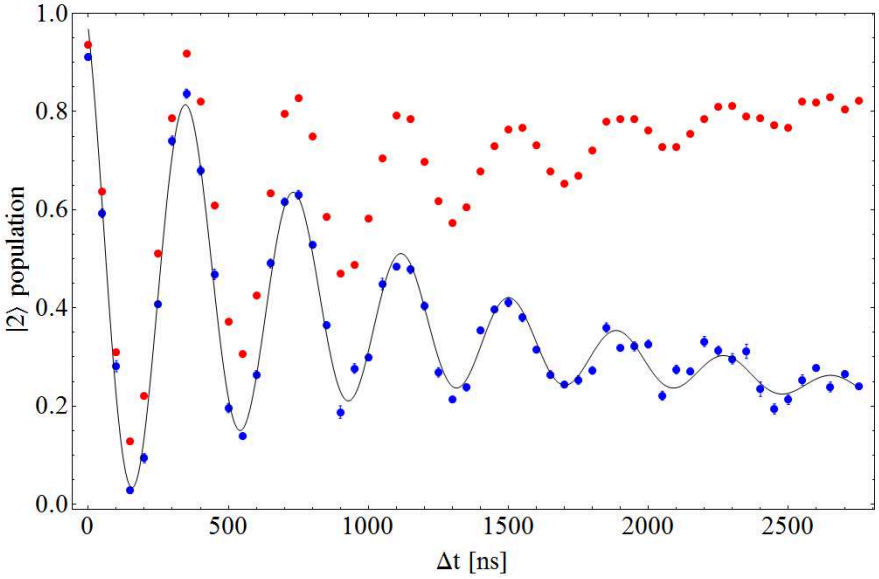

Figure 5.2: Two population readout (red) and three population readout (blue) of Ramsey data. A fit for the blue points of the form (5.1) is also shown.

The second excited state population is fitted automatically using a function of the form

$$p_2(\Delta t) = \left(y + A\, e^{-\Delta t/T^*_{2,2}} \cos(\omega_{Ramsey}\, \Delta t - \phi)\right) e^{-\Delta t/T_{1,2}} \tag{5.1}$$

Note, that $T^*_{2,2}$ is the averaged dephasing time of state $|2\rangle$.[1] This characteristic time for the qutrit is obtained from the fit and written to the pulse pattern configuration file. To fit different sets of experimental data, the initial value of the fit parameters has to be extracted from the data. Thereby, the same method as in [Men13] is used. The initial values of y and A are set as the minimum population and the difference of the maximum and the minimum population, respectively. From the position and complex phase of the largest Fourier component, the starting values of ω_{Ramsey} and ϕ are given. The initial value of $T_{1,2}$, is extracted from the pulse pattern configuration file.
The obtained oscillation frequency ω_{Ramsey} is given by the difference of the detuned drive frequency (RF) $\tilde{\omega}_{1,2}$ to the real transition frequency $\omega_{1,2}$. Thus, the IF frequency to drive the transition on resonance can be determined. Note that if one is only interested in a rather crude value of the Ramsey frequency, a two population reconstruction might be sufficient.

When executing the above calibration routine in the experiment, we often observed prominent contributions to the frequency spectrum from more than one frequency component. This problem especially arises, when the system is not optimized for the usage of the artificial atoms as qutrits. To identify the additional frequency components, besides the Ramsey fringes, a frequency spectrum is added to the log file.

In Section 3.2, a two frequency Ramsey measurement was presented. The only difference in the data analysis compared to the analysis explained above is that a simultaneous fit of the data for two different detunings within one data set is used. Thereby, the data set is fitted for both cases in Figure 3.2. The transition frequency is then determined using the fit which has the smaller sum of the absolute value of the fit residuals. This method was successfully tested. Note, that as above three level population reconstruction should be used for a precise data analysis.

5.2 π and $\pi/2$ amplitudes for $|1\rangle \leftrightarrow |2\rangle$ transition

For the Rabi pulse sequence of Section 3.3, Rabi oscillations of the $|0\rangle$ and $|2\rangle$ populations depending on the pulse amplitude ϵ can be observed (see Figure 5.3).
The oscillation of the second excited state population is fitted automatically with a function of the

[1] The time scale for the loss of phase information of state $|2\rangle$ is given by the dephasing time $\frac{1}{T_{2,2}} = \frac{1}{2T_{1,2}} + \frac{1}{T_{\phi,2}}$. $T_{1,2}$ is the energy relaxation time (see Section 3.5) and $T_{\phi,2}$ the pure dephasing time, which is due to fluctuations of the qutrit transition frequencies. As the Ramsey data is obtained from an average over a large number of equivalent measurements, fluctuations of the transition frequencies are contained in the average. Thus, the measured dephasing time $T^*_{2,2}$ is smaller than $T_{2,2}$ [Bau12].

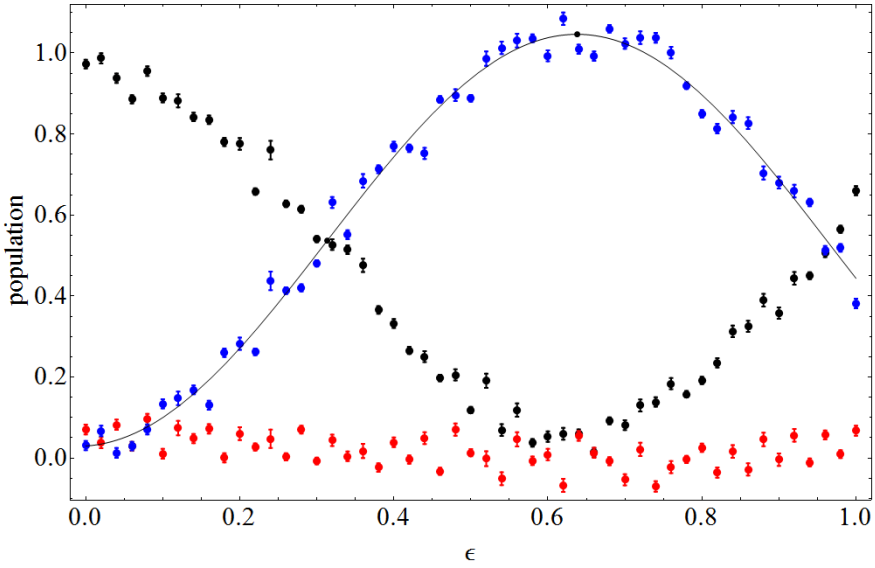

Figure 5.3: Three level population readout of Rabi pulse sequence with the ground (black), first excited (red) and second excited (blue) state populations. The second excited state population is fitted with a function of the form (5.2).

form

$$p_2(\epsilon) = y + A\,\cos(\omega_{Rabi}\,\epsilon - \phi) \tag{5.2}$$

using the same method to determine the starting values of the fit parameters as for the Ramsey measurement. From this fit, the π and $\pi/2$ amplitudes can be extracted.
In contrast to the data from the Ramsey measurement, there is no decay of population to the first excited state. The reason is, that the maximum duration of the Ramsey pulse sequence is about a factor 1000 larger than the length of the Rabi sequence, which consists of a single one-qubit pulse. As the first excited state population can be neglected, a two level readout can can be used for the data analysis.

5.3 DRAG parameter for for $|1\rangle \leftrightarrow |2\rangle$ transition

In Section 3.4 the procedure to shape the pulses was explained. Experimental data from such a DRAG calibration routine is depicted in Figure 5.4. Note, that due to the short pulse sequence, a two level readout was used. At the optimal value of q_{scale}, the curves of the three populations should intersect. The approximate position of this point can be found by fitting two populations with a linear function.
The population for the pulse sequence $\pi/2_x \cdot \pi_x$ (blue points in Figure 5.4) depends on q_{scale}. This dependence is unexpected, as there is only one rotation axis for this pulse sequence and thus there

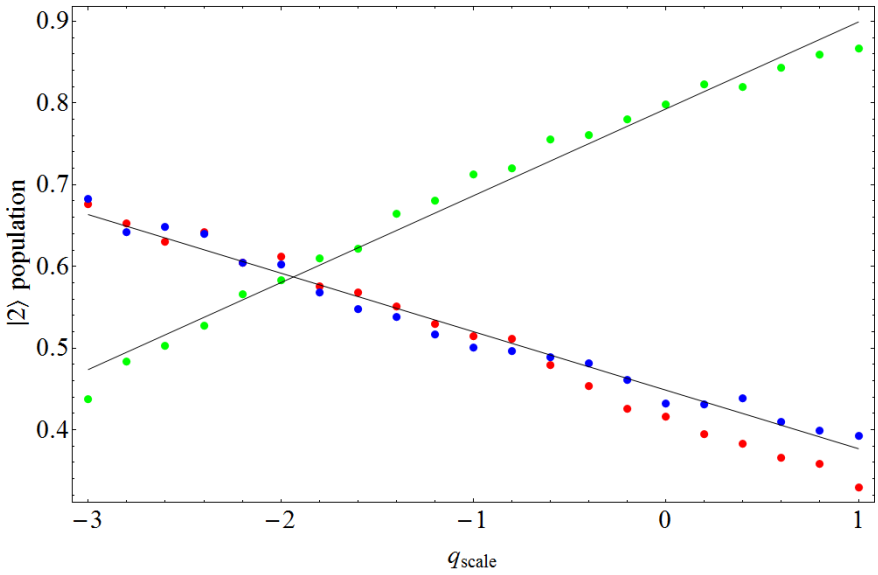

Figure 5.4: Experimental data for DRAG pulse calibration. The value of q_{scale} is varied for different pulse combinations $\pi/2_x \cdot \pi_x$ (blue), $\pi/2_x \cdot \pi_y$ (green), $\pi/2_x \cdot \pi_{-y}$ (red). Two populations are fitted with a linear function

should no dependence on an additional phase that the effective two level system acquires. When the data was recorded, the right sideband at about 100 MHz from the LO frequency was used to drive the $|0\rangle \leftrightarrow |1\rangle$ transition. For the $|1\rangle \leftrightarrow |2\rangle$ transition, the left sideband with an offset of about 200 MHz from the LO (see Figure 5.5) was used. For this frequency configuration, there is a weak component from the $|0\rangle \leftrightarrow |1\rangle$ drive at the $|1\rangle \leftrightarrow |2\rangle$ transition, as the mixer is not purely linear. We think, that this is the main reason for the behavior observed in Figure 5.4.
Although no proper value for q_{scale} could be determined in the experiment, we could demonstrate, that the routine is properly implemented for the usage with the calibration software.

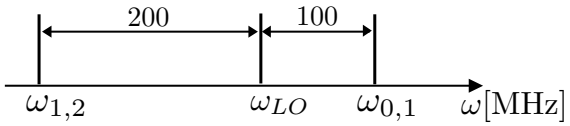

Figure 5.5: Frequency scheme for up-conversion at the mixer

5.4 CalTom for $|1\rangle \leftrightarrow |2\rangle$ transition

Experimental results from the CalTom pulse sequence are depicted in Figure 5.6. The data was analyzed with a two level readout.

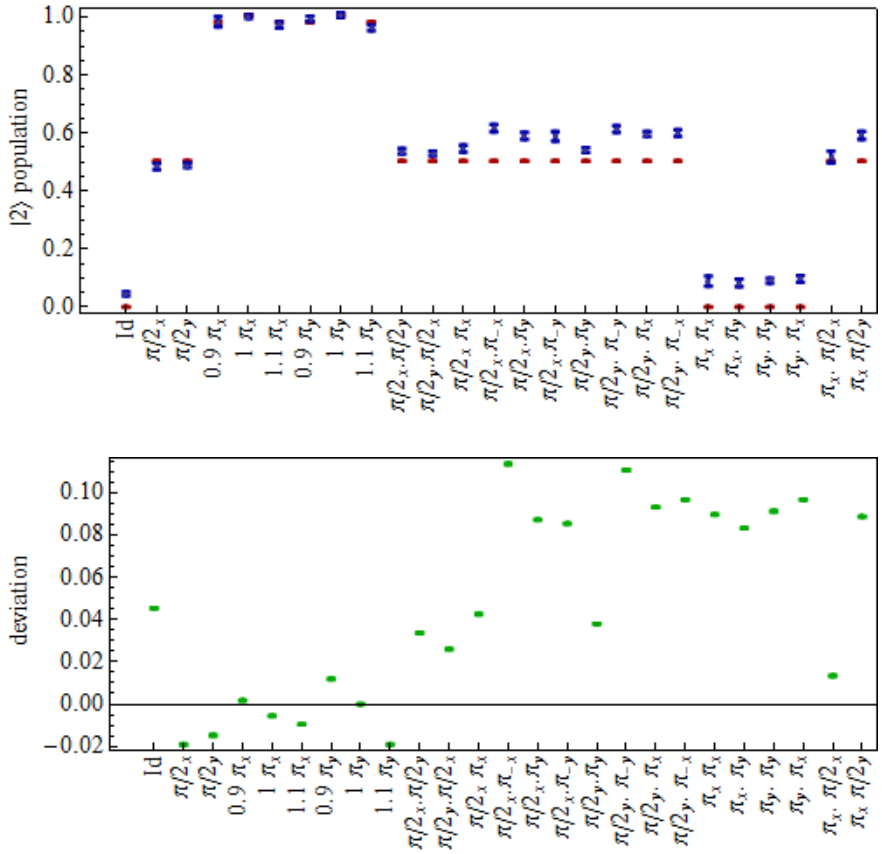

Figure 5.6: Experimental data for CalTom pulse sequence. The expected population is marked in red. The lower plot shows the deviation of the measured from the theoretical population.

As the DRAG calibration of the pulses did not work properly (see Section 5.3), there are strong deviations of the experimental populations from the theoretically expected values.
Still, the software for the routine works properly.

5.5 Energy relaxation time

As it was discussed in Section 3.5, the $|1\rangle$ population of the qubit decays as a function of the delay Δt. This decay can be modeled with a function of the form $A\,e^{-\Delta t/T_{1,1}}$. By fitting this function to experimental data as in Figure 5.7, an energy relaxation time of about 2.5 μs is obtained.

To model the decay of the second excited state population, the decay channels $|2\rangle \rightarrow |1\rangle$ and

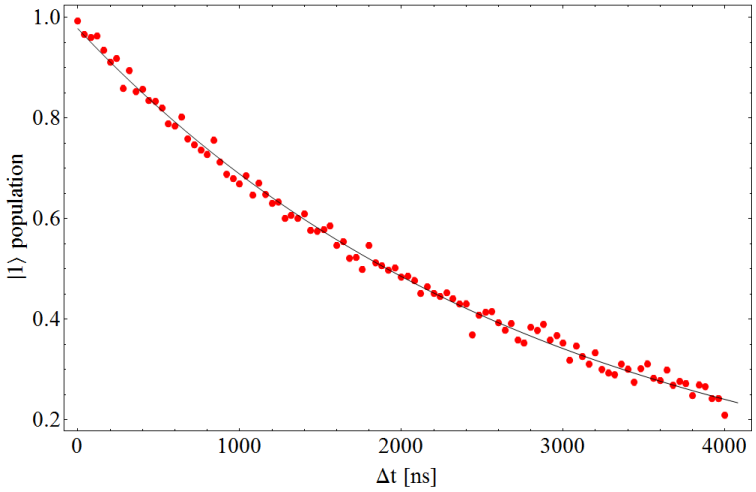

Figure 5.7: Experimental data for energy relaxation measurement of qubit with a fit for the exponential decay.

$|1\rangle \rightarrow |0\rangle$ must be considered. Hence, the fit has to be of the form

$$p_2(\Delta t) = A\, e^{-\Delta t/T_{1,2}} + B\left(1 - e^{-\Delta t/T_{1,2}}\right) e^{-\Delta t/T_{1,1}} \tag{5.3}$$

To automatically fit this function to experimental data, the starting value for $T_{1,1}$ is extracted from a measurement on the qubit (see above). An exemplary file exported from the analysis script is depicted in Figure 5.8. Three population read out has to be used due to the same reasons as for the Ramsey sequence. Typically measured energy relaxation times are comparable to the qubit case.

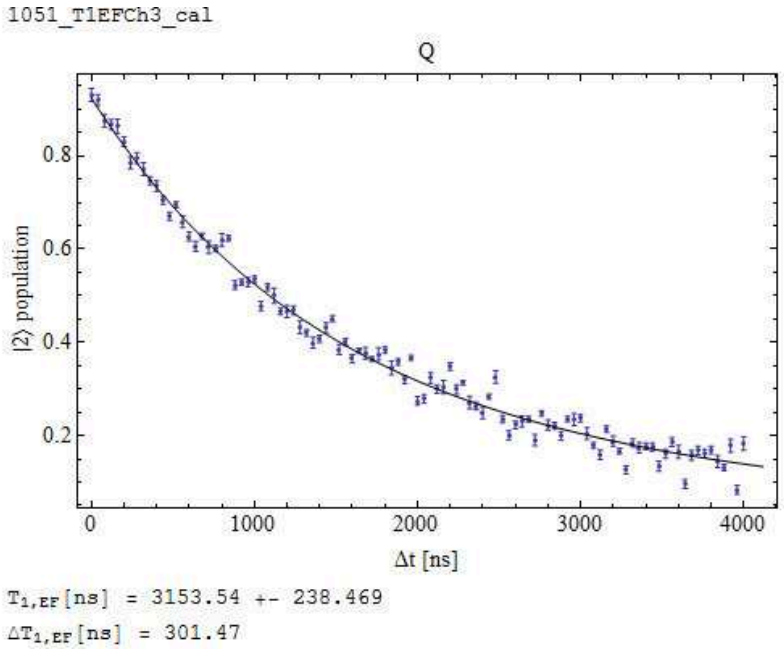

Figure 5.8: Analysis file output for energy relaxation measurement on second excited state population. Data is fitted with a function of the form given by Equation 5.3.

Chapter 6

Conclusion

In this thesis, a software for the automatic calibration of the $|0\rangle \leftrightarrow |1\rangle$ and $|1\rangle \leftrightarrow |2\rangle$ transition of superconducting transmons was presented. This software generalizes an already existing program from [Men13], such that arbitrary single qubit and qutrit gate operations can be added without the need for *LabVIEW* programming. The generalization was possible using a new data flow, for which *LabVIEW* is no longer directly involved in the data analysis. The data flow could be implemented using the communication of *Mathematica* with *LabVIEW* via the standard output and an .ini file, that is exchanged between *LabVIEW* and *Mathematica*. Also it was necessary, that new calibration parameters are written from *Mathematica* to the pulse pattern configuration files.
Besides this generalization, handling of *Mathematica* errors was implemented and the graphical user interface has several new useful features.
Compared to the previous version, also new calibration routines were added. This includes routines for the calibration of pules resonant with the $|1\rangle \leftrightarrow |2\rangle$ transition. Also routines to determine the energy relaxation times of the excited qutrit states and to extract the transition frequencies for large drive detuning were added. In the end, the functionality of the software was successfully tested.

Acknowledgements

I want to thank Prof. Andreas Wallraff for giving me the opportunity to conduct my semester thesis in his group. A big thanks to Yves Salathé and Markus Oppliger for their assistance and support. Thanks also to Johannes Heinsoo for the good collaboration. Finally I want to appreciate the help of Philipp Kurpiers, Christian Lang and Lars Steffen.

Bibliography

[Bau12] Baur, Matthias: *Realizing Quantum Gates and Algorithms*, ETH Zurich, Diss., 2012

[BDD+02] Bremner, Michael J. ; Dawson, Christopher M. ; Dodd, Jennifer L. ; Gilchrist, Alexei ; Harrow, Aram W. ; Mortimer, Duncan ; Nielsen, Michael A. ; Osborne, Tobias J.: Practical Scheme for Quantum Computation with Any Two-Qubit Entangling Gate. In: *Phys. Rev. Lett.* 89 (2002), S. 247902

[Bia10] Bianchetti, Romeo: *Control and readout of a superconducting artificial atom*, ETH Zurich, Diss., 2010

[DCG+09] DiCarlo, L. ; Chow, J. M. ; Gambetta, J. M. ; Bishop, Lev S. ; Johnson, B. R. ; Schuster, D. I. ; Majer, J. ; Blais, A. ; Frunzio, L. ; Girvin, S. M. ; Schoelkopf, R. J.: Demonstration of two-qubit algorithms with a superconducting quantum processor. In: *Nature* 460 (2009), S. 240–244

[DOS+12] Dewes, A. ; Ong, F. R. ; Schmitt, V. ; Lauro, R. ; Boulant, N. ; Bertet, P. ; Vion, D. ; Esteve, D.: Characterization of a Two-Transmon Processor with Individual Single-Shot Qubit Readout. In: *Physical Review Letters* 108 (2012), Nr. 5

[Gro96] Grover, L.: A fast quantum mechanical algorithm for database search. In: *Proceedings of the twenty-eighth annual ACM symposium on Theory of computing*, ACM, 1996, S. 212–219

[KYG+07] Koch, Jens ; Yu, Terri M. ; Gambetta, Jay ; Houck, A. A. ; Schuster, D. I. ; Majer, J. ; Blais, Alexandre ; Devoret, M. H. ; Girvin, S. M. ; Schoelkopf, R. J.: Charge-insensitive qubit design derived from the Cooper pair box. In: *Phys. Rev. A* 76 (2007), S. 042319

[Men13] Menke, T.: *Realizing a calibration program for superconducting qubits.* ETH Zurich, Semester thesis, 2013

[MGRW09] Motzoi, F. ; Gambetta, J. M. ; Rebentrost, P. ; Wilhelm, F. K.: Simple Pulses for Elimination of Leakage in Weakly Nonlinear Qubits. In: *Phys. Rev. Lett.* 103 (2009)

[SSO+13] Steffen, L. ; Salathe, Y. ; Oppliger, M. ; Kurpiers, P. ; Baur, M. ; Lang, C. ; Eichler, C. ; Puebla-Hellmann, G. ; Fedorov, A. ; Wallraff, A.: Deterministic quantum teleportation with feed-forward in a solid state system. In: *Nature* 500 (2013), S. 319–322

[WSB+04] Wallraff, A. ; Schuster, D.I. ; Blais, A. ; Frunzio, L. ; Huang, R.-S. ; J.Majer ; Kumar, S. ; Girvin, S. M. ; Schoelkopf, R. J.: Strong coupling of a single photon to a superconducting qubit using circuit quantum electrodynamics. In: *Nature* 431 (2004), S. 162–167

ETH

Eidgenössische Technische Hochschule Zürich
Swiss Federal Institute of Technology Zurich

Declaration of originality

The signed declaration of originality is a component of every semester paper, Bachelor's thesis, Master's thesis and any other degree paper undertaken during the course of studies, including the respective electronic versions.

Lecturers may also require a declaration of originality for other written papers compiled for their courses.

I hereby confirm that I am the sole author of the written work here enclosed and that I have compiled it in my own words. Parts excepted are corrections of form and content by the supervisor.

Title of work (in block letters):

Software for arbitrary single qubit & qutrit gate calibration

Authored by (in block letters):

For papers written by groups the names of all authors are required.

Name(s):	**First name(s):**
Landig	Andreas

With my signature I confirm that

- I have committed none of the forms of plagiarism described in the 'Citation etiquette' information sheet.
- I have documented all methods, data and processes truthfully.
- I have not manipulated any data.
- I have mentioned all persons who were significant facilitators of the work.

I am aware that the work may be screened electronically for plagiarism.

Place, date	**Signature(s)**
Munich, 26.04.2014	Landig

For papers written by groups the names of all authors are required. Their signatures collectively guarantee the entire content of the written paper.